# The BLAST Experiment[☆]

D. Hasell[f,*], T. Akdogan[f], R. Alarcon[a], W. Bertozzi[f], E. Booth[b], T. Botto[f], J.R. Calarco[i], B. Clasie[f], C. Crawford[f], A. DeGrush[f], K. Dow[f], D. Dutta[d], M. Farkhondeh[f], R. Fatemi[f], O. Filoti[i], W. Franklin[f], H. Gao[1], E. Geis[a], S. Gilad[f], W. Hersman[i], M. Holtrop[i], E. Ihloff[f], P. Karpius[i], J. Kelsey[f], M. Kohl[f], H. Kolster[f], S. Krause[f], T. Lee[i], A. Maschinot[f], J. Matthews[f], K. McIlhany[h], N. Meitanis[f], R. Milner[f], J. Rapaport[g], R. Redwine[f], J. Seely[f], A. Shinozaki[f], A. Sindile[i], S. Širca[f], T. Smith[c], S. Sobczynski[f], M. Tanguay[f], B. Tonguc[a], C. Tschalaer[f], E. Tsentalovich[f], W. Turchinetz[f], J.F.J. van den Brand[k], J. van der Laan[f], F. Wang[f], T. Wise[j], Y. Xiao[f], W. Xu[d], C. Zhang[f], Z. Zhou[f], V. Ziskin[f], T. Zwart[f]

[a] *Arizona State University, Tempe, AZ 85287*
[b] *Boston University, Boston, MA 02215*
[c] *Dartmouth College, Hanover, NH 03755*
[d] *Duke University, Durham, NC 27708-0305*
[e] *Johannes Gutenberg-Universität, 55099 Mainz, Germany*
[f] *Massachusetts Institute of Technology, Cambridge, MA 02139 and MIT-Bates Linear Accelerator Center, Middleton, MA 01949*
[g] *Ohio University, Athens, OH 45701*
[h] *United States Naval Academy, Annapolis, MD 21402*
[i] *University of New Hampshire, Durham, NH 03824*
[j] *University of Wisconsin, Madison, WI 53706*
[k] *Vrije Universitaet and NIKHEF, Amsterdam, The Netherlands*

---

**Abstract**

The BLAST experiment was operated at the MIT-Bates Linear Accelerator Center from 2003 until 2005. The detector and experimental program were designed to study, in a systematic manner, the spin-dependent electromagnetic interaction in few-nucleon systems. As such the data will provide improved measurements for neutron, proton, and deuteron form factors. The data will also allow details of the reaction mechanism, such as the role of final state interactions, pion production, and resonances to be studied. The experiment used: a longitudinally polarized electron beam stored in the South Hall Storage Ring; a

[☆] Work supported by the United States Department of Energy under Cooperative Agreement DE-FC02-94ER40818.

[*] Corresponding author
*Email addresses:* hasell@mit.edu (D. Hasell)

highly polarized, isotopically pure, internal gas target of hydrogen or deuterium provided by an atomic beam source; and a symmetric, general purpose detector based on a toroidal spectrometer with tracking, time-of-flight, Čerenkov, and neutron detectors. Details of the experiment and operation are presented.
*Key words:* BLAST, storage ring, polarized target, polarized beam, tracking detector, Čerenkov detector, scintillator detector
*PACS:* 29.20.Dh, 29.25.Pj, 29.27.Hj, 29.40.Gx, 29.40.Ka, 29.40.Mc

---

## 1. Introduction

BLAST (Bates Large Acceptance Spectrometer Toroid) refers to the detector, collaboration, and the experimental program which was carried out to study in a comprehensive and systematic manner the spin-dependent electromagnetic interaction in few nucleon systems [1, 2]. The primary goal was improved measurements of nucleon form factors and the structure of few nucleon systems. However, the data should also test our understanding of the spin-dependent reaction mechanism at momentum transfers below 1 GeV/c and permit studies of final state interactions, pion production, the role of resonances, etc.

The experiment combined several highly specialized systems and procedures to accomplish its goals, namely:

1. An electron beam with an energy of 850 MeV and polarization of $\sim 66\%$ was stored in the South Hall Ring of the MIT-Bates Linear Accelerator Center. Currents of over 200 mA with lifetimes more than 25 minutes were typical. A Siberian Snake in the storage ring opposite the BLAST experiment maintained the longitudinal polarization at the target and a Compton Polarimeter monitored the polarization of the stored beam.
2. An atomic beam source was used to produce a highly polarized proton (vector) or deuteron (vector and tensor) target. The polarized gas was injected into an open-ended, thin-walled tube, aligned with the beam and centered at the interaction point, thus providing an isotopically pure, polarized target without entrance or exit windows, minimizing background.

3. A left/right symmetric, large acceptance, general purpose detector was designed to identify and measure the scattered particles. The detector incorporated drift chambers within a toroidal magnetic field to measure the momentum, vertex position, and scattering angles of the charged particles. Aerogel Čerenkov detectors were used to help distinguish electrons from pions. Time-of-flight scintillator bars measured the relative arrival timing of particles and provided the timing signal to trigger the data acquisition electronics. Thick scintillators were used to detect neutrons. A multi-level, general purpose trigger and buffered data acquisition system allowed data to be accumulated for different reaction channels concurrently and at high rates.
4. The symmetric design and operation of the experiment minimized systematic errors. The helicity of the electron beam was reversed for each fill of the ring (approximately every 10 minutes). The various polarization states (vector for protons, vector and tensor for deuterons) were changed randomly every five minutes. An extensive slow control and monitoring system recorded the status of the beam, target, and detector throughout the experiment as well as automated the interaction of accelerator, target, detector, and data acquisition during the experimental running.
5. Finally, the physics analyses using the data accumulated are based on spin asymmetry measurements where uncertainties in beam current, target density, and detector efficiency cancel to first order.

The following sections describe the various components of the BLAST experiment in greater detail and provide information on its operation.

## 2. The MIT-Bates Linear Accelerator

The MIT-Bates Linear Accelerator Center is situated in Middleton, MA, USA and, during the BLAST experiment, was operated by MIT on behalf of the United States Department of Energy. A schematic layout of the facility is shown in Figure 1. The facility included a polarized electron source followed by

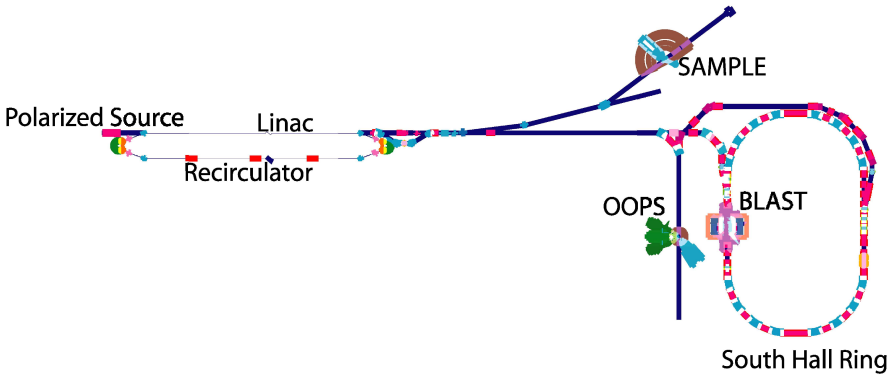


Figure 1: Schematic layout of the MIT-Bates Linear Accelerator Center.

a 500 MeV linear accelerator with a recirculator. Accelerated beams could be directed to the North Hall, as was done for the SAMPLE [3, 4, 5] experiment, or into the South Hall. In the South Hall the beam could be used either directly or injected into the South Hall Storage Ring, SHR. The SHR in turn could be operated in storage mode or used as a beam stretcher where the beam was resonantly extracted into an external beamline, as was done for the OOPS Experiment [6]. During the BLAST experiment the SHR was operated in storage mode with long-lived circulating beams.

The following two subsections describe:

- the production of the polarized electron beam and its injection and storage in the South Hall Ring, and
- the Compton polarimeter located just upstream of the BLAST experiment, used to monitor the polarization of the electron beam in the ring.

### *2.1. Polarized Electron Beam*

Polarized beams at MIT-Bates were generated through photoemission based on the excitation of selective transitions in a GaAs cathode using circularly polarized light [7, 8]. The polarized source employed a very stable fiber-coupled diode array laser system [9] which produced peak power up to 250 W at 808 ±

3 nm with a highly versatile pulse structure. The light was circularly polarized by a straightforward system of polarizers and waveplates optimized for this wavelength and directed onto the surface of a strained GaAs photocathode residing in an ultra-high vacuum gun structure. The photocathode was a high-gradient-doped $GaAs_{0.95}P_{0.05}$ photocathode designed to produce peak polarization at 810 nm [10]. This combination yielded an electron beam with high polarization and comfortably met peak intensity requirements for filling the South Hall Ring.

Photocathodes were certified prior to installation on the accelerator column using a 60 keV Mott polarimeter [11]. During normal operation, the polarization from the source was periodically monitored with a 20 MeV transmission polarimeter [12] located in the early stages of the linac. This provided a rapid measurement of the beam polarization at low energies based on analysis of bremsstrahlung from a beryllium oxide target. The transmission polarimeter was calibrated with respect to the SAMPLE Møller polarimeter, which provided polarization measurements at higher energies with an absolute uncertainty of approximately 5%. These steps generally ensured that the beam polarization from the source was at least 70%.

The polarized injector beamline contained a Wien filter which allowed the beam polarization to be rotated to the desired orientation for injection into the South Hall Ring. A remotely controlled half-wave plate in the laser optics was inserted or removed from the laser system to alternate the beam helicity each time the SHR was filled.

Polarized electrons from the source could be accelerated to energies up to 1 GeV by the Bates linac and recirculator [13] for injection into the SHR. Because electrons circulated in the SHR for a long time following a ring fill, the source was operated so as to produce beam only during intervals when filling the storage ring (i.e. 15–20 s every ∼10–20 minutes during BLAST operation) to prolong the operational lifetime of the photocathode. Even during these filling intervals the duty cycle was quite low as the laser was pulsed at rates below 10 Hz, a limit based on the 100 ms damping time for electrons entering the

South Hall Ring. The laser power was kept at a level to produce a 2 mA peak current in the linac. The pulse structure of the laser was adjusted to produce pulses of electrons with 1.6 $\mu$s width, which were shortened to 1.3 $\mu$s by slits near the beginning of the recirculator. The slits removed the first 0.3 $\mu$s of the accelerated pulse. To produce a short rise time of the beam-pulse, compensating for beam-loading transients in the accelerator cavities, the RF pulse in one of the transmitters was delayed through a pin-diode, which effectively lowered the energy for this 0.3 $\mu$s by $\sim 40$ MeV, and this part of the beam was intercepted by the slits. The 1.3 $\mu$s pulse length was chosen to match the transit time of electrons in the accelerator plus recirculator, as the accelerator was run using a head-to-tail scheme in which electrons from the front of the recirculated pulse followed immediately behind those on the trailing edge of the pulse from the buncher.

The pulse length also reflected the transit time for electrons to circulate the South Hall Ring (190 m circumference) exactly twice. This matched the length of the accelerator plus the recirculator up to the point where the beam was injected into the accelerator for its second pass. Electrons emerging from the accelerator/recirculator were stacked in the SHR using two-turn injection at full energy, thus adding 4 mA to the ring with each accelerator pulse. The storage ring followed a race track design with 16 dipoles and two long straight sections for experiments. A single RF cavity in the northern arc of the SHR compensated for synchrotron losses. The ring RF frequency was 2856 MHz, producing a beam with 1812 buckets distributed over its 190 m circumference, making the stored beams effectively continuous wave. Beams circulated at a frequency of 1.576 MHz in the SHR.

The high frequency for electron circulation allowed a very high average current on target to be generated by a relatively small number of stored electrons. Typically stored currents in excess of 200 mA were achieved and over 300 mA have been stored for short periods of time. The current was continuously monitored by the SHR's Direct Current Current Transformer (DCCT). The lifetime of the beam in the SHR was governed by a number of conditions including

vacuum, target thickness, and the position of apertures such as halo slits. In the absence of a target, lifetimes greater than 45 minutes were typical, limited by quantum lifetime. However, during normal operation of the BLAST target, lifetimes around 25 minutes were typical.

The electron beam was injected into the SHR with longitudinal polarization at the BLAST target. The BLAST detector was located in the west straight section of the SHR, immediately downstream of the injection region. The stored beam had a strong waist at this point, and the injected beam had a cross-over. This ensured the target cell was not struck while stacking current into the ring. Four scintillators were mounted as beam halo monitors around the beam-pipe downstream of the BLAST interaction region and were used to optimize the beam transport to minimize the background during the experiment. Across the ring in the eastern straight section was a solenoidal full Siberian Snake which imparted a rotation of 180° about the beam axis to the electron polarization vector. This rotation effectively constrained the stable spin direction for the SHR to be oriented longitudinally at the BLAST experiment. It also eliminated spin diffusion, thereby preserving the polarization of properly oriented beams. The polarization lifetime of the SHR was measured to be more than 1000 minutes for most beam energies and thus was much longer than the beam lifetime.

### *2.2. Compton Polarimeter*

Measurements of the polarization of the electron beam stored in the SHR were provided by a Compton back-scattering polarimeter [14]. The polarimeter was based on the spin dependence in the energy distribution of circularly polarized photons scattered from longitudinally polarized electrons [15]. The design was strongly influenced by other devices which have operated in a comparable energy range, particularly the NIKHEF Compton polarimeter [16] at the Amsterdam Pulse Stretcher (AmPS) Ring.

The polarimeter included a 5 W, 532 nm continuous-wave solid-state laser. The light was circularly polarized by a Pockels cell which permitted rapid helicity control. A series of remotely controlled mirrors enabled the laser beam

to intersect the electron beam with a crossing angle of less than 2 mr in the SHR's northwest arc upstream of the BLAST interaction region (Figure 2). The Compton back-scattered photons were then detected in a CsI calorimeter.

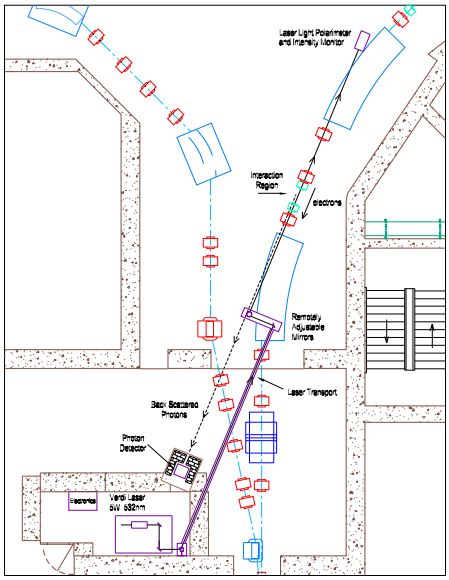


Figure 2: Schematic showing the layout of the Compton polarimeter just upstream of the BLAST detector.

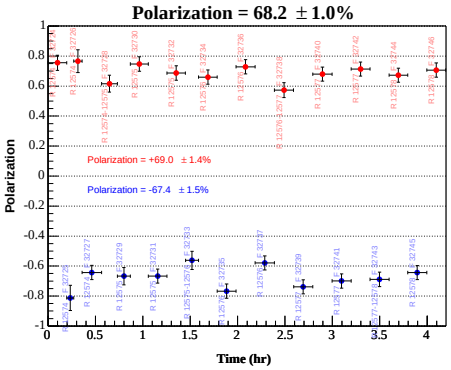


Figure 3: Example of typical online results from measuring the beam helicity over several fills of the storage ring.

The polarization of the laser was reversed at 9 Hz and the asymmetry in the energy distribution of the back-scattered photons was analyzed to determine the longitudinal polarization of the electron beam. A correction was applied to account for the spin precession of the electron beam between the measurement made by the Compton polarimeter and the BLAST interaction region.

At energies below 1 GeV the polarization asymmetry in Compton scattering is only a few percent and steps were taken to minimize both statistical and systematic uncertainties. Background due to bremsstrahlung from the target was minimized by locating the polarimeter upstream of the BLAST internal target region. The background was measured continually during the experiment with the aid of a rotating chopper wheel which could block the laser beam from

intercepting the electron beam. A movable Pb collimator was used to define the acceptance of the calorimeter and to minimize background from beam halo. The readout of the calorimeter was designed to permit linear operation at high rates and the phototube bases were engineered to minimize saturation effects. Furthermore, a set of stainless steel absorbers could be inserted remotely to attenuate the photon flux observed at the highest electron beam currents. This permitted the polarimeter to operate over a wide range of beam currents ranging from a few mA to 250 mA. The polarization of the electron beam in a given fill was usually measured to a statistical precision of around 4% (Figure 3).

The mean longitudinal polarization of the beam during the 2004 BLAST experiment was $P_e = 0.66 \pm 0.04$. The uncertainty was dominated by systematic uncertainty in the calibration of the polarimeter. The magnitude of polarization for the two electron helicity states was the same to better than 1%. This was verified with the aid of an RF dipole developed to flip adiabatically the helicity of the stored beam within a fill [17] and helped constrain geometric false asymmetries in the polarimeter. Although the efficiency in flipping the spin reached 98%, this device introduced additional dead time to the experiment as well as problems with beam stability at high currents. For this reason, it was used only occasionally during BLAST operation and reversal of the electron beam helicity was generally performed at the polarized source prior to each SHR fill.

## 3. The Atomic Beam Source Internal Target

An atomic beam source [18] (ABS) was used to produce highly polarized, isotopically pure protons and deuterons in the BLAST target cell aligned with the electron beam in the South Hall Ring. The ABS was originally designed and built at NIKHEF [19, 20] but most components were redesigned at MIT-Bates to accommodate the BLAST environment: primarily the space limitations and the 2 kG magnetic field in which the ABS was situated.

The ABS, schematically shown in Figures 4 and 5, consisted of:

- an RF dissociator which produced atomic hydrogen or deuterium from the

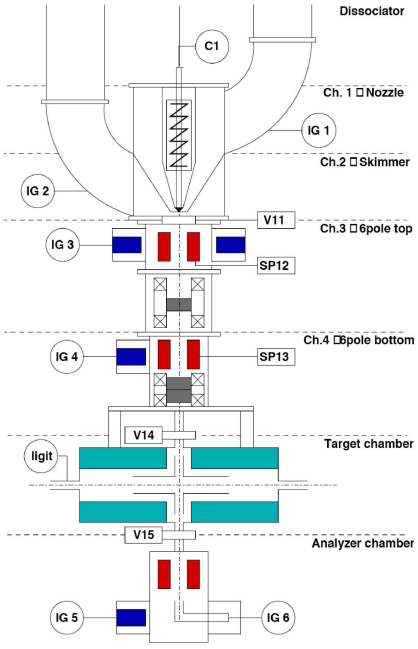


Figure 4: Schematic of the BLAST atomic beam source, the internal target, and Breit-Rabi polarimeter.

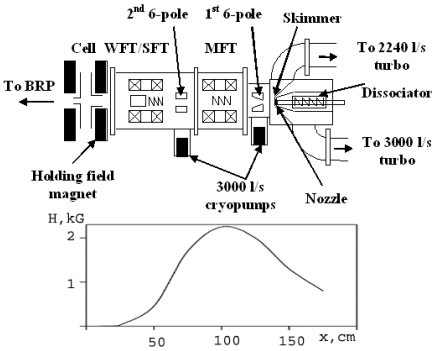


Figure 5: Location of the ABS elements relative to the magnetic field in which each operated.

molecular gas,

- four turbo-molecular pumps used to pump the region directly after the dissociator,
- two sets of permanent sextupole magnets which focused the atomic beam into the target tube located on the beam axis,
- three RF transition units in combination with magnets to populate selectively the desired polarization states, and
- a Breit-Rabi polarimeter located below the target cell, used to tune and optimize the ABS transitions.

During operation $\sim$ 1 mbar L/s of hydrogen or deuterium gas was flowed through the dissociator. A cold head (70 K) at the exit of the dissociator

cooled the nozzle and reduced recombination. A small flow of oxygen ($\sim$ 0.001 mbar L/s) was added to produce a thin layer of ice on the nozzle which formed after 1–2 h and improved dissociation. After approximately 1 week of operation the accumulation of ice would block the nozzle. The nozzle would then be warmed up to room temperature to melt the ice, and then cooled down again. This process took 5–7 h.

The nozzle had to be replaced approximately every 3 weeks when operated with deuterium because sputtering produced a residue on the inside of the nozzle. With hydrogen the nozzle was operated for 2 months without this problem. Each time the nozzle was replaced its position had to be optimized to maximize the intensity of polarized atoms injected into the target cell.

Each sextupole magnet consisted of 24 permanent magnets in a cylindrical array. The pair of sextupole magnets was positioned so that atoms with electron spin $+\frac{1}{2}$ entering the first magnet would be efficiently transported ($\approx 50\%$) to the target cell while atoms with $-\frac{1}{2}$ electron spin would not (0%). Atoms with electron spin $-\frac{1}{2}$, after transition in the intervening MFT unit, had only a 4% probability of reaching the target cell after passing through the second sextupole.

The three RF transition units consisted of the medium field transition unit, MFT, located between the sextupole magnets, and the weak and strong field transition units, WFT and SFT, located after the second sextupole magnet. The MFT produced $\pi$-transitions using a time-varying magnetic field (gradients up to 10 G/cm) perpendicular to a static magnetic field (30–40 G) plus an RF coil operated at 30 MHz for deuterium and 60 MHz for hydrogen. The WFT and SFT shared the same magnet. However, depending on the transitions desired, only one of the WFT or SFT was operated. The WFT RF was operated at 8 and 12 MHz, respectively, for deuterium and hydrogen and required a field of just a few Gauss, which was therefore sensitive to external fields. The SFT was only used for deuterium but required 420 MHz RF, necessitating a special silver-plated cavity to reduce losses. It also employed a magnetic field of 63 G for $2 \rightarrow 6$ transitions (see below) or 141 G for $3 \rightarrow 5$.

The hyperfine structures for hydrogen and deuterium are shown in Figure 6. Only the upper states ($m_S = +\frac{1}{2}$) pass through the first sextupole magnet. For

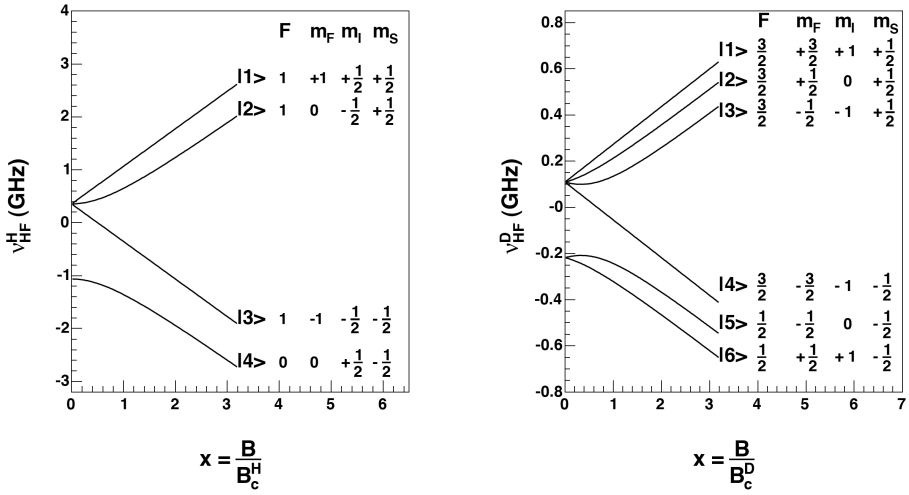


Figure 6: Hyperfine structure of hydrogen (left) and deuterium (right) as a function of the reduced magnetic field ($B_c^H = 507$ G, $B_c^D = 117$ G)

hydrogen the MFT would induce the $2 \rightarrow 3$ transition and only state $|1\rangle$ would be transported to the target cell. The WFT following the second sextupole, could then be used (or not) to induce the transition $1 \rightarrow 3$ thus selecting the nuclear polarization for the hydrogen atoms delivered to the target cell. For deuterium the MFT induced either $3 \rightarrow 4$ or $1 \rightarrow 4$ transitions and then either the SFT (inducing either $2 \rightarrow 6$ or $3 \rightarrow 5$) or the WFT ($1, 2 \rightarrow 3, 4$) would be used to achieve the desired, nuclearly polarized, deuteron states in the target cell.

The polarization states used during the experiment and the schemes for operating each unit are given in Tables 1 and 2. For hydrogen the experiment cycled randomly, but evenly, through the two polarization states, $V+$ and $V-$. For deuterium the experiment cycled randomly, but evenly, through three polarization states: one purely tensor, $T-$, and the other two being combinations of vector and tensor polarization. This permitted both vector and tensor asymmetries to be measured efficiently and simultaneously by combining the spin-

| Name | V+ | V- |
|---|---|---|
| MFT | $2 \rightarrow 3$ | $2 \rightarrow 3$ |
| States | $\|1\rangle$ | $\|1\rangle$ |
| WFT | off | $1 \rightarrow 3$ |
| State | $\|1\rangle$ | $\|3\rangle$ |
| $P_Z$ | +1 | -1 |

Table 1: Transition schemes and resulting polarization states for hydrogen.

| Name | V+ | V- | T- |
|---|---|---|---|
| MFT | $3 \rightarrow 4$ | $3 \rightarrow 4$ | $1 \rightarrow 4$ |
| States | $\|1\rangle$, $\|2\rangle$ | $\|1\rangle$, $\|2\rangle$ | $\|2\rangle$, $\|3\rangle$ |
| WFT | off | $1,2 \rightarrow 3,4$ | off |
| SFT | $2 \rightarrow 6$ | off | $3 \rightarrow 5$ |
| States | $\|1\rangle$, $\|6\rangle$ | $\|3\rangle$, $\|4\rangle$ | $\|2\rangle$, $\|5\rangle$ |
| $P_Z$ | +1 | -1 | 0 |
| $P_{ZZ}$ | +1 | +1 | -2 |

Table 2: Transition schemes and resulting polarization states for deuterium.

dependent yields appropriately. The spin state was changed every 5 minutes during the experiment.

The ABS was situated above the BLAST interaction point between the vertical coils of the BLAST toroid. One of the major challenges for operating the ABS was the external magnetic field which reached values up to 2.2 kG in the region of the MFT (see Figure 5). This required extensive shielding of the ABS and careful tuning and monitoring of the transition units to correct for hysteresis in the ABS magnets.

To assist in tuning the transitions, a Breit-Rabi polarimeter with a dipole magnet was installed below a small aperture in the target cell. The dipole magnet transported atoms into one of three compression tubes (left, middle, and right) depending on their spin state. This permitted the relative populations of the atomic polarization states and the degree of dissociation to be sampled and thus optimized.

The target tube was 60 cm long and 1.5 cm in diameter centered on the beam axis. The tube walls were made from 50 $\mu$m aluminum and had open ends to eliminate background that would be produced by the electron beam passing through any entrance or exit windows. The target cell was also cooled to around 100 K and coated with Drifilm to reduce depolarization inside the target cell. A thick tungsten collimator with 1 cm diameter aperture was situated just

upstream of the target cell and served to protect the cell walls from the beam halo and the injection flash during filling.

In addition to the ABS, an unpolarized gas system with a well-determined buffer volume could be connected to the target cell. The unpolarized system was used to make systematic checks of false asymmetries. Also, by measuring the pressure change in the buffer volume (at constant temperature), the flow, and thus the density, of unpolarized gas in the target cell could be determined using the known conductance of the target cell. Comparing the scattering rates observed with unpolarized to polarized or ABS running permitted the target density with the ABS to be measured.

The intensity of polarized atoms in the target cell was very sensitive to the pumping in the ABS. Four turbomolecular pumps operated directly on the volume around the nozzle and cryopumps were used in the region of the sextupole magnets. Also, turbomolecular pumps connected to the beamline before and after the target cell were used to isolate the target from the high vacuum of the beamline and thus minimize the effect of the target on beam lifetime.

A holding field magnet around the target cell was used to define the nominal spin direction at the center of the target cell. During the experiment the spin angle was determined from the measured tensor asymmetry in elastic *ed* scattering to be $31.3^\circ \pm 0.43^\circ$ in 2004 and $47.4^\circ \pm 0.45^\circ$ in 2005, relative to the beam direction, and horizontal into the left sector. The nominal spin directions were chosen so electrons scattering into the left sector corresponded to momentum transfers roughly perpendicular to the target spin direction, while electrons scattering into the right sector had momentum transfers roughly parallel to the target spin. The spin direction varied slightly along the length of the target cell (see Figure 7). This was measured by a variety of techniques which yielded a consistent shape. A parameterization of this shape was used in the analyses with the value at the center of the target determined from the physics analysis of elastic scattering from tensor polarized deuterium [21].

Assuming a beam polarization of 66%, polarizations of $P_Z \approx 83\%$ were achieved for hydrogen and $P_Z \approx 89\%$ (79%) and $P_{ZZ} \approx 69\%$ (55%) for deu-

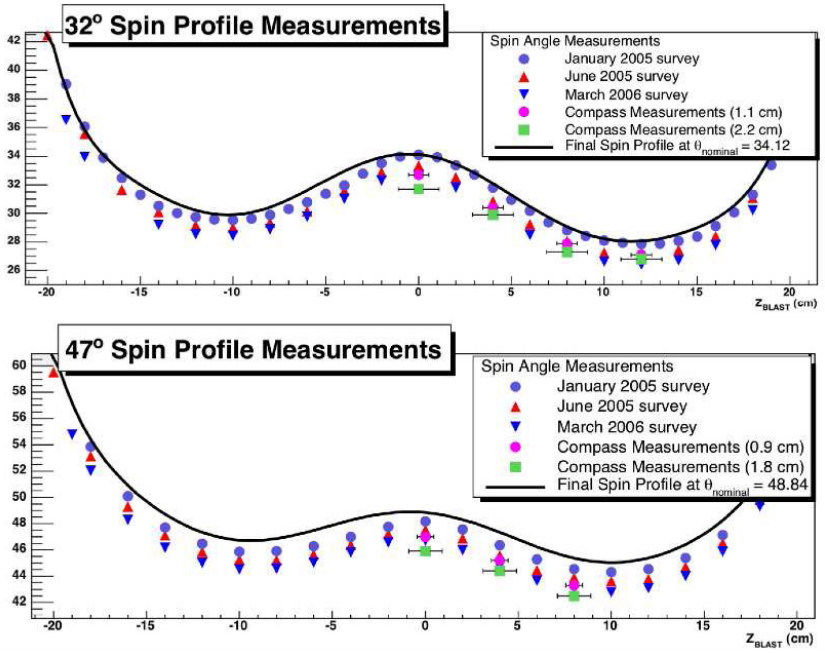


Figure 7: Polarization direction (polar angle in degrees) as a function of position along the target cell.

terium in 2004 (2005). Target areal densities around $7 \times 10^{13}$ atoms/cm$^2$ for both hydrogen and deuterium were typical.

## 4. The BLAST Detector

The BLAST detector (see Figure 8) was situated on the South Hall Ring just downstream of the injection point. The detector was based upon an eight sector, toroidal, magnetic field. The two horizontal sectors were instrumented with detector components while the two vertical sectors were used by the internal targets and pumping for the beamline. The detector was left/right symmetric with the exception of the neutron detectors which were enhanced in the right sector (see Section 4.5). Each sector included drift chambers for tracking, aerogel Čerenkov detectors to discriminate between electrons and pions, time-of-flight scintillators to determine the relative timing of the reaction products

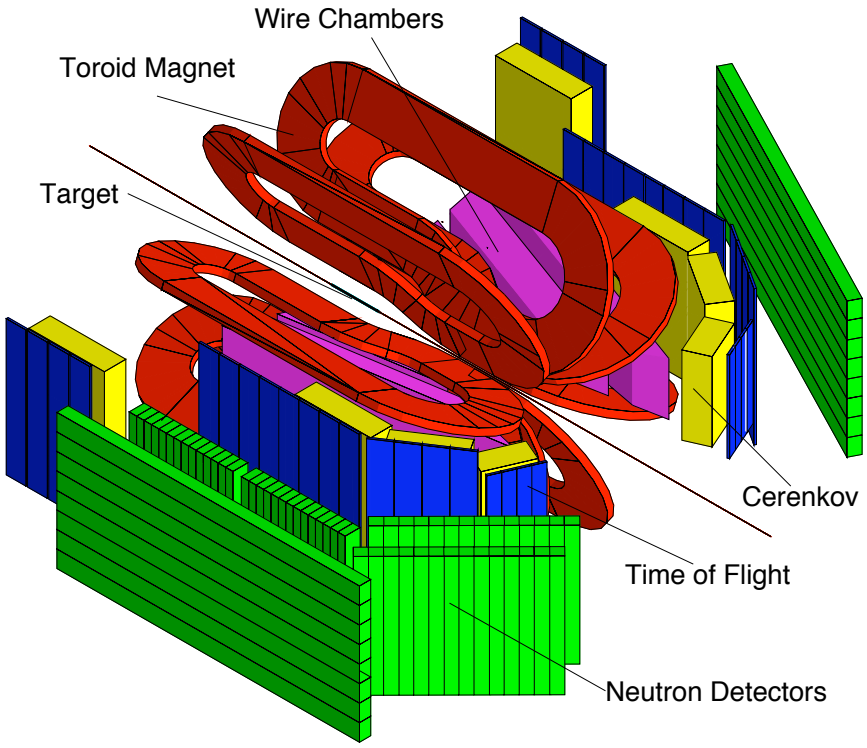


Figure 8: Schematic of the BLAST detector showing the main detector elements.

and provide the trigger timing, and thick walls of plastic scintillators to identify neutrons using time-of-flight. The following sections describe the detector components in greater detail.

### *4.1. Toroidal Magnet*

The toroidal magnet was designed and assembled at MIT-Bates. A toroidal configuration was chosen to ensure a small field along the beamline to minimize effects on the beam transport, and also to have small gradients in the region of the target cell. The magnetic field in the region of the drift chambers was used to identify the charge and momentum-analyze the charged particles produced during the experiment. It also minimized the number of low-energy charged particles reaching the detectors.

The toroid consisted of eight copper coils placed symmetrically about the beamline. Their profile and nominal position relative to the beam line and target are shown in Figure 9. The unusual shape extended the intense region of

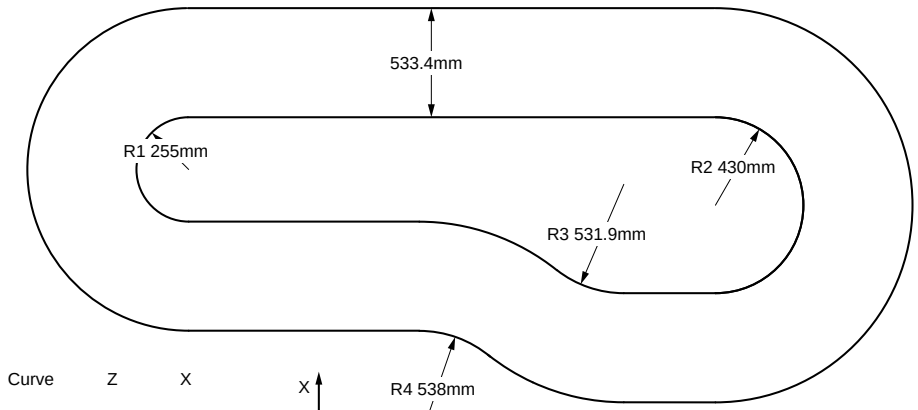


| Curve | Z | X |
|---|---|---|
| R1 | -636.3 | 1288.4 |
| R2 | 1938.5 | 1113.4 |
| R3 | 1491.0 | 1215.5 |
| R4 | 491.0 | -38.5 |

Figure 9: Plan view of BLAST coil outline showing dimensions and position relative to the center of the target cell.

the toroidal magnetic field to forward angles. Each coil consisted of 26 turns of hollow, 1.5 inch square copper tube organized into two layers of 13 turns. The copper tubes were wrapped with fiberglass tape and then potted with epoxy resin. The coils were cooled by flowing water through the hollow conductors. During the BLAST experiment the normal operating current was 6730 A, resulting in a maximum field of about 3.8 kG.

Before the detectors were installed, the magnetic field was carefully measured particularly along the beam axis and in the target region [22]. The coil positions were adjusted to minimize the field along the beamline and gradients at the target. After this was done a systematic mapping was performed of the magnetic field in each of the horizontal sectors throughout the volume which would be occupied by the tracking detector. The results of this mapping were compared with results from a simple calculation based on the Biot-Savart law as well as a

Vector Fields[1] TOSCA simulation.

Discrepancies between the measured and calculated field values could be explained by the uncertainty in the precise conductor positions and by the deflection of the coils under gravity or when energized. The Biot-Savart calculations were redone allowing the coil positions to move radially, along the beam direction, and in azimuthal position to obtain good agreement with the measured values. These calculated values were then used to extend the mapping to regions where it was impossible to make a direct measurement. This extended mapping was used in the reconstruction of events.

### *4.2. Drift Chambers*

The drift chambers measured the momenta, charges, scattering angles, and vertices for the particles produced in the reactions studied with BLAST. This was done by tracking the charged particles in three dimensions through the toroidal magnetic field and reconstructing the trajectories. Measuring the curvature of the tracks yielded the particles' momenta, and the directions of curvature determined their charge. Tracing the particles' trajectories through the mapped magnetic field back to the target region allowed the scattering angles, polar and azimuthal, to be determined. The position of closest approach to the beam axis was taken as the vertex position for the event.

To maximize the active area, the drift chambers were designed to fit between the coils of the toroidal magnet such that the top and bottom plates of the drift chamber frame were in the shadow of the coils as viewed from the target. The drift chambers had a large acceptance and nominally subtended the polar angular range 20°–80° and ±15° in azimuth with respect to the horizontal plane, and were orientated such that 73.54° with respect to the beam was perpendicular to the face of the chambers. Because of these choices the chambers were trapezoidal in shape (see Figure 10).

Each sector in BLAST contained three drift chambers (inner, middle, and

[1] Vector Fields Inc. Aurora, IL, USA

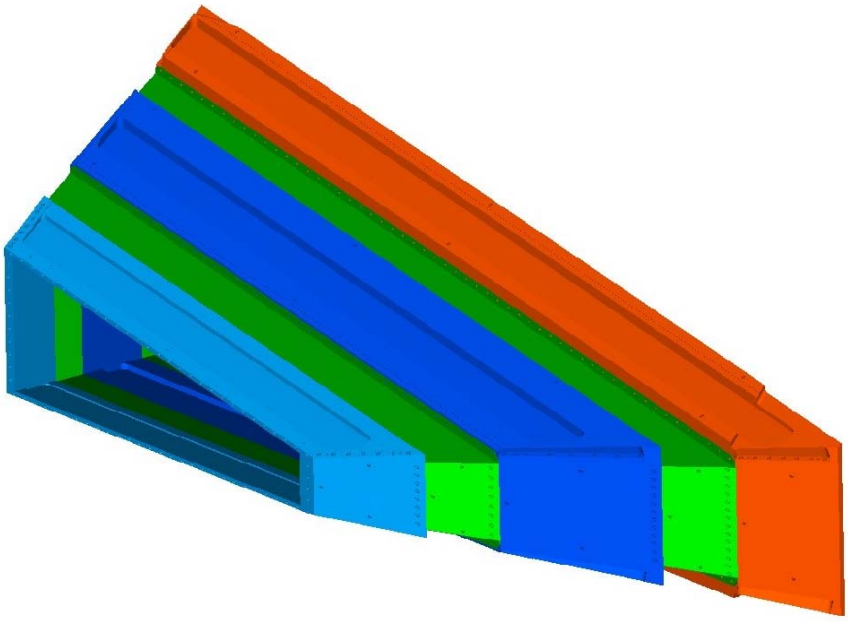

Figure 10: Isometric view of all three drift chambers assembled into a single gas volume.

outer) joined together by two interconnecting sections to form a single gas volume. This was done so that only a single entrance and exit window was required for the combined drift chambers, thus minimizing energy loss and multiple scattering.

Each of the three chambers consisted of top, bottom, and two end plates. Each plate was precisely machined from a solid aluminum plate[2] and then pinned and bolted together to form each drift chamber. The positions of the feedthrough holes (described below) and twelve (12) tooling balls set in inserts along the length of the top and bottom plates were measured with a coordinate measuring machine, CMM, at Allied Mechanical. These data were used for quality assurance and for the alignment of the chambers in BLAST. The chambers were then disassembled and shipped to MIT, where they were cleaned

[2]Allied Mechanical Ltd., Ontario, CA, USA

and reassembled to form the individual chambers. O-rings were used to form a gas seal. The chambers were wired (described below) separately and then the three chambers of a sector and the interconnection sections were assembled to form the complete drift chamber for each sector.

The top and bottom plates of the two interconnecting sections between the chambers were $\frac{1}{8}$ inch aluminum sheets to be flexible and to conform to the shape of the connected chambers. The end pieces of the interconnection sections were rigid and connected to the chambers with pins and bolts to hold the relative positions of the three drift chambers.

Figure 11 shows a cross sectional view of the top plates for the three drift

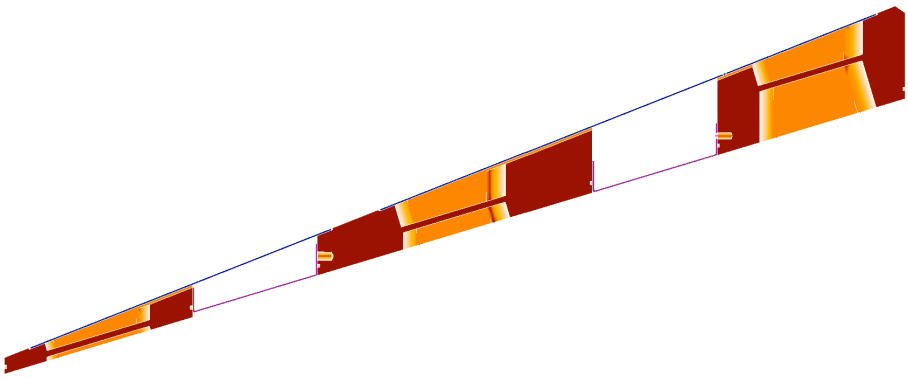

Figure 11: Cross sectional view of the top plates of the three drift chambers and the two interconnecting sections when assembled into a single gas volume.

chambers when assembled. The darker shade shows the top plates for the three chambers. The lighter shade is used to highlight the recesses which were machined into both sides of each plate to produce a 7 mm thick section to accommodate the feedthroughs for the wires which formed the drift chamber cells. The thick portions of each plate were needed to resist the combined wire tensions over the length of the drift chamber. Recall that the top and bottom plates of the frame were in the shadow of the coil as viewed from the interaction area so the thicknesses shown here did not impact on the detector acceptance. The frame dimensions were adjusted so that each chamber bowed by approxi-

mately the same amount (on the order of 1 mm) due to the wire tension. This was necessary to simplify connecting the chambers into a single gas volume. The thin aluminum profile which formed the interconnecting section is visible along the bottom edge between pairs of chambers. The empty region above the interconnecting plate was used to hold the amplifier/discriminator electronics, HV distribution, and for the HV and signal cable runs. The thin line running along the top of the whole assembly represents a $\frac{1}{8}$ inch copper sheet which was used to protect the feedthroughs, wires, and electronics. The bottom plates for the chambers and interconnecting sectors were similar and also had a protective copper plate.

Each chamber consisted of two super-layers (or rows) of drift cells separated by 20 mm. The drift cells were "jet-style" formed by wires. Figure 12 shows a

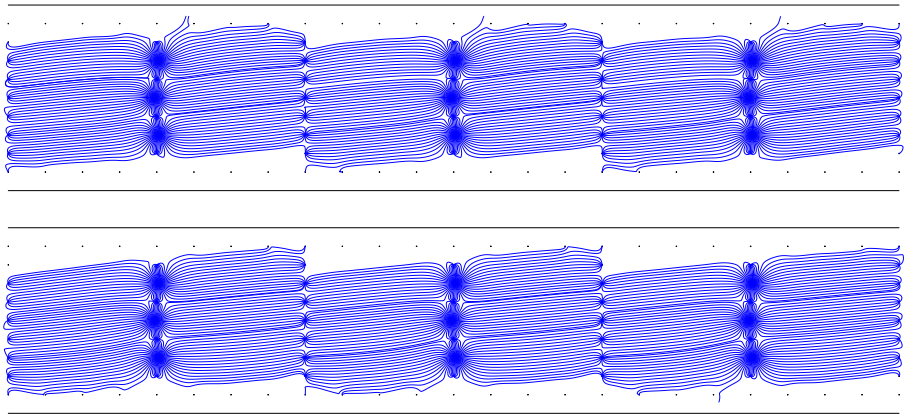

Figure 12: Portion of a chamber showing the two super-layers of drift cells formed by wires. Lines of electron drift in the drift cells assuming the maximum BLAST field of 3.8 kG are also shown.

portion of one chamber with the two super-layers of drift cells formed by wires. It also shows characteristic "jet-style" lines of electron drift in a magnetic field. Each drift cell was $78 \times 40$ mm$^2$ and had 3 sense wires staggered $\pm 0.5$ mm from the center line of each cell to help resolve the left/right ambiguity in determining position from the drift time. This pattern of wires was realized by stringing wires

between the top and bottom plates of each chamber. Holes for each wire were machined in the thin plate of the recessed areas of the top and bottom plates to accept Delrin feedthroughs. The feedthrough had a gold plated copper tube insert through which the wire was strung and crimped. The pin provided a convenient connector for the HV.

Machining the feedthrough holes was nontrivial. The wires for each super-layer were inclined at $\pm 5^\circ$ to the vertical. This stereo angle between the front and back super-layers in each chamber allowed reconstruction in three dimensions. Because of this the hole patterns in the top and bottom plates were not mirror images but were shifted relative to each other. This was further complicated by the fact that the recessed plate surface was inclined both left to right and front to back and the hole direction was not perpendicular to either. The feedthrough holes first had to be spot faced and then drilled and reamed to produce a press fit for the feedthrough.

Each drift chamber was wired separately. First, the chamber had to be pre-stressed to the tension that all the wires would exert. This was done by stringing piano wire through the centre of each drift cell and tensioning these to the total tension which the real wires would produce. The tension was determined by plucking the piano wire and measuring the frequency using a microphone connected to a computer which performed a Fourier analysis. This process was repeated until all piano wires were properly tensioned. Next, $\frac{1}{4}$ inch clear plastic windows were attached to the front and rear faces of the chamber. This helped keep the insides of the chamber clean and also protected the wires from accidents. The chambers were then moved into a clean room for the actual wiring.

The chambers were wired horizontally. First a wire was strung through a feedthrough. Then the wire was fastened to a long, hollow stainless steel needle which was threaded through the holes machined in the top and bottom plates. Pulling the needle through carried the wire from one side to the other where it was threaded through another feedthrough. Then the feedthroughs were pushed into the machined holes. The wire was drawn through the feedthroughs from

the supply spool to ensure only clean and straight wire was used. Then the copper pin of the feedthrough was crimped on one side securing the wire. A weight was attached to the wire on the other side and stretched over a pulley. The other pin was then crimped. This process was repeated from one end of the chamber to the other removing the piano wires as each cell was completed.

Periodically the tensions in the real wires were checked. This was done by passing DC electrical currents through two neighboring wires. An AC current was added to one producing an alternating magnetic field in which the other wire would start to vibrate. Then the AC current was switched off, and the current induced by the vibrating wire measured and Fourier analyzed to determine the frequency. Generally two frequencies were measured, one for each wire; but by measuring different pairs and by the different strengths of the signals, it was possible to identify each wire's frequency and hence tension.

When all three chambers of a sector were wired the plastic protective windows were removed and the interconnecting sections installed to join the three chambers into a single unit. Then the electrical connections were made and amplifier/discriminator electronics installed.

The completed drift chamber was then optically surveyed. The twelve tooling ball locations on the top and bottom plates of each individual chamber were measured to determine the relative positions of the three chambers with respect to each other. Survey targets in bushings on the end plates of all chambers were also measured.

The drift chamber was then mounted in the sub-detector frame and its position and orientation adjusted until it was in its nominal position. This position was checked with another optical survey of the targets on the end plates. These data were used together with the previous survey and the data from the CMM data on the hole positions to determine the position of each sense wire in the BLAST coordinate system.

With all three drift chambers assembled and positioned, there were 18 planes of sense wires in each sector with which to track the charged particles produced at BLAST. In total there were approximately 10,000 wires with 954 sense wires

for both sectors in BLAST.

A helium:isobutane gas mixture (82.3:17.7) was chosen for the drift chambers. The chambers were maintained at a pressure of approximately 1 inch of water above atmospheric pressure with a flow rate of around 3 L/min. The primarily helium mixture had a relatively low density to reduce multiple scattering and energy loss. Also, because the BLAST toroidal field was inhomogeneous over the tracking volume, a small Lorentz angle was desirable so that corrections were small even in regions with high magnetic fields. The helium gas mixture chosen satisfied this as well with $\approx 7^\circ$ Lorentz angle in a 3.8 kG field. Figure 12 shows the distinctive lines of electron drift, "jets", for this cell design at 3.8 kG. Using a single gas volume minimized the number of entrance and exit windows for the same reason. Two layers of 25 micron mylar were used for the entrance and exit windows.

### *4.3. Čerenkov detectors*

Immediately behind the drift chambers in each sector were aerogel Čerenkov detectors [23] designed and produced at Arizona State University to identify electrons up to 700 MeV/c with 89% efficiency. These detectors were used to discriminate between pions and electrons which otherwise were not clearly separated by timing in BLAST. An aerogel Čerenkov detector was chosen to produce a compact detector and to minimize the energy loss.

Originally there were four Čerenkov detectors in each sector. A schematic of a Čerenkov box is shown in Figure 13. The boxes contained the aerogel and supported shielded photomultiplier tubes, PMTs, at both the top and bottom. The front and back faces of the boxes were made of honeycomb sandwiched between 1 mm thick aluminum to minimize material while providing support for the PMTs. The sides were made of $\frac{1}{8}$ inch aluminum sheets. The inside of each box was painted with Spectraflect[3], a white, diffusively reflective paint which has 96–98% reflectivity for light at a wavelength of 600 nm.

[3]Labsphere, North Sutton, NH, USA

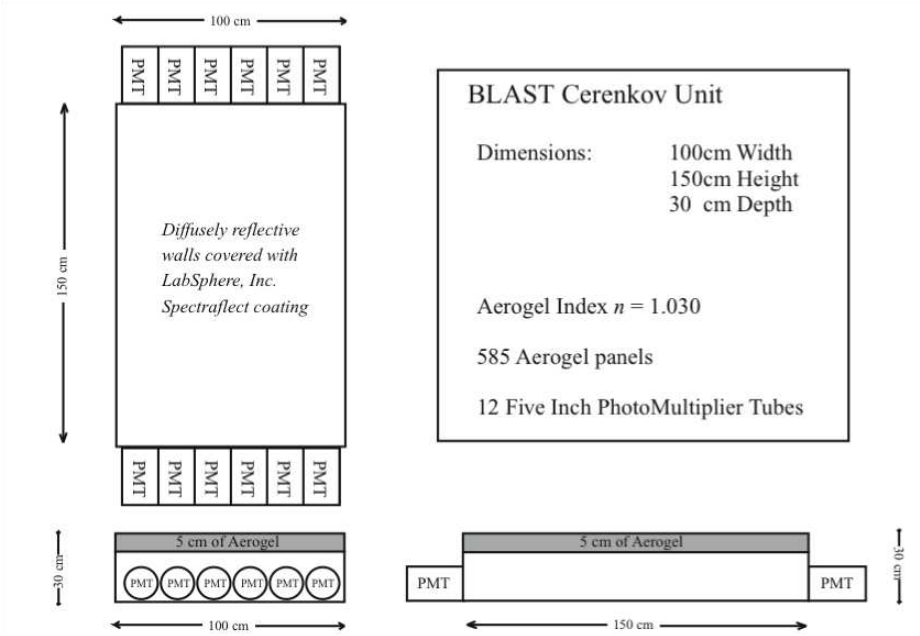


Figure 13: Schematic of a Čerenkov detector box which contained the aerogel and supported the photomultiplier tubes.

A clear silica aerogel[4] was used. The tiles were approximately $11 \times 11 \times 1$ cm$^3$ and were laid in rows separated by a strip of mylar (a razor was used to trim the tiles so they fit snugly). The forward Čerenkov detectors in each sector had 7 layers of aerogel tiles with a refractive index of $n = 1.020$ while the other detectors had 5 layers and an index of $n = 1.030$. The layers of aerogel were held in place by a thin mylar foil. A photograph of the inside of a detector box is shown in Figure 14.

The forward-most detector box in each sector had 6 PMTs (3 top, 3 bottom) while the next had 8 PMTs and the rear two boxes each had 12 PMTs. Five-inch Photonis[5] photomultipliers, XP4500B, were used to collect the Čerenkov radiation.

[4]Matsushita Electric Works, Ltd. Osaka, Japan
[5]Photonis USA Inc. Sturbridge, MA, USA

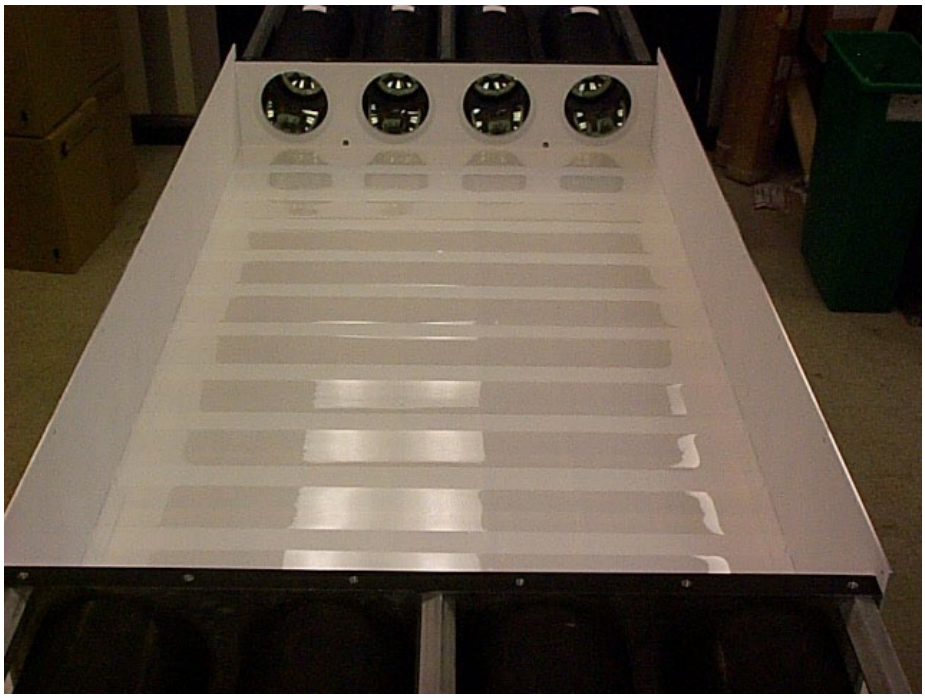

Figure 14: Inside view of Čerenkov detector showing white painted box with aerogel and openings for four PMTs.

The photomultiplier tubes chosen were sensitive to magnetic fields above 0.5 G. The initial shielding design had two concentric iron cylinders of 10 mm and 6 mm wall thickness separated by an air gap around each tube. However, measurements inside the cylinders at the location of the PMTs showed a residual magnetic field on the order of 3–5 G when the BLAST toroid was energized. Extra iron plates 0.5 inch thick in the forward region and 1 inch thick in the backward region had to be added between the BLAST toroid and the PMT enclosures to adequately shield the tubes from the toroid's fringe field.

During the experiment the rearmost box in each sector was removed to improve the detection of elastically scattered deuterons with the time of flight scintillators. This fourth box from each sector was used for the BAT detector (see 4.6). With the remaining three boxes in each sector, an electron identification efficiency of 89% was achieved.

*4.4. Time-of-Flight Scintillators*

In each sector 16 vertical scintillator bars formed the time-of-flight (TOF) detector. The TOF detector was designed and produced at the University of New Hampshire to provide a fast, stable timing signal correlated with the time of each event at the target independent of which scintillator bar was struck. This signal was used to trigger the readout and data acquisition system for all other components and particularly provided the COMMON STOP signal for the drift chambers. This permitted relative timings among all components to be measured. The TOF detector also provided a measure of energy deposition to aid particle identification. Approximate position information was also possible from the timing difference between the top and bottom photomultiplier tubes.

The TOF detector curved behind (see Figure 15) the wire chambers and

Figure 15: TOF detector mounted in sub-detector support during assembly.

Čerenkov detectors in each sector, roughly matching the angular coverage of the tracking detector in both polar ($\sim 20^\circ < \theta <\sim 80^\circ$) and azimuthal ($\pm \sim 15^\circ$)

projections. The forward four bars at $\theta < 40^\circ$ were 119.4 cm high, 15.2 cm wide, and 2.54 cm thick. The remaining 12 bars at $\theta > 40^\circ$ were 180.0 cm high, 26.2 cm wide, and 2.54 cm thick.

Bicron[6] BC-408 plastic scintillator was chosen for its fast response time (0.9 ns rise time) and long attenuation length (210 cm). Each TOF scintillator bar was read out at both ends via Lucite light guides coupled to 3-inch diameter Electron Tubes[7] model 9822B02 photomultiplier tubes equipped with Electron Tubes EBA-01 bases. The light guides were bent to point away from the interaction region so the PMTs would be roughly perpendicular to the toroidal magnetic field. Mu-metal shielding was used around all PMTs. The bases had actively stabilized voltage dividers so that the timing was independent of the gain.

With readout from both ends of a TOF scintillator bar, the time difference provided coarse position information. To provide a timing signal independent of position along the TOF, the signals from each PMT were split, with one part from each pair of tubes going to a meantimer. This meantime signal was used to provide the event timing signal. Because each TOF was at a different distance from the target center, a delay was added to the closer detectors corresponding to the time for a relativistic particle to travel the difference in distance. These time differences were measured for each sector by inserting a thin plastic scintillator paddle near the target chamber and measuring the TOF detector timing relative to the common start from this paddle. These delayed, meantimed signals were thus correlated with the time of the event at the target. The signals from each PMT were also distributed to TDCs and ADCs.

A 2 mm thick Pb foil was placed in front of each TOF bar to attenuate X-rays from the target region. It also prevented back-scattered radiation from firing the Čerenkov detector and being mis-identified as electrons. However, the Pb foil was removed from the four rearmost TOF scintillator bars to improve

[6]Bicron, Solon, OH, USA

[7]Electron Tubes Ltd, Ruislip, Middlesex, England

the sensitivity to low-energy deuterons.

Gains for the PMTs were set by requiring the ADC signal for minimum ionizing particles from cosmic rays to peak in channel 1250. An intrinsic time resolution of $320 \pm 44$ ps was measured for the 32 TOF detectors, which was significantly better than the 500 ps required by the experiment. Timing offsets between pairs of scintillator bars were determined using cosmic rays periodically during the experiment and monitored continuously using the laser flasher system (section 4.7). The efficiency was determined to be better than 99%.

*4.5. Neutron Detectors*

Beyond the other detectors were banks of thick scintillator to detect neutrons. Three types of neutron detector were employed in BLAST:

**Ohio Walls -** Two walls approximately $10 \times 180 \times 400$ cm$^3$ situated in both left and right sectors. Each wall was made using 10 cm thick, 22.5 cm high, 400 cm long bars of scintillator stacked horizontally with PMTs at either end.

**LADS15 -** Two walls approximately $15 \times 213 \times 160$ cm$^3$, one behind the other at approximately 35° in the right sector. Each wall was made of 14 wedge shaped scintillator bars, 15 cm thick, 14.5 cm wide (at midpoint of wedge), and 160 cm high arranged vertically with PMT readout at each end. A solid wall was formed by alternating the direction of the wedges.

**LADS20 -** Two walls approximately $20 \times 137.2 \times 160$ cm$^3$positioned parallel to the beamline, in front of the Ohio wall in the right sector. Each wall was made of 14 wedge shaped scintillator bars, 20 cm thick, 9.8 cm wide (at midpoint of wedge), and 1.6 m high arranged vertically with PMT readout at each end. A solid wall was formed by alternating the direction of the wedges.

The Ohio Walls were designed and produced at Ohio University using Bicron-408 scintillator as used in the TOF detector. Similarly the same 3 inch PMTs and bases as in the TOF detector were used here.

The LADS scintillators were originally produced for the Large Acceptance Detector System [24] at the Paul Scherrer Institute, Switzerland and obtained from the Jefferson Laboratory, Virginia, USA. Hamamatsu,[8] 5-inch PMTs were used to read out the LADS scintillator bars. Bases were developed at MIT-Bates and UNH with active, transistor-based compensation for the last four dynodes which permitted a power supply with lower maximum current to be used. These actively compensated bases had a more stable gain ($\pm$5–10%) at rates up to 800 kHz compared to the usual passive bases ($\sim$ 100% variation).

The neutron detectors were initially gain-matched using cosmic rays and a dedicated trigger. Later the detection threshold was estimated using the 2.2 MeV endpoint of a $^{90}$Sr beta spectrum. For the Ohio Wall this yielded a threshold of approximately 2.5 MeV for electrons corresponding to 6–7 MeV for protons. A threshold less than 1 MeV (2.5 MeV) for electrons was obtained for the 20 cm (15 cm) thick LADS detectors corresponding to approximately 4 MeV (7 MeV) for protons.

A VME-based logic module was developed at MIT-Bates to process the raw signals from the LADS detectors. This featured leading-edge discrimination with a prompt and delayed output for each channel, which were connected to the scalers and TDCs. It also generated a logical AND of top and bottom PMT pairs with a flexible delay and an OR of all the AND signals which could be used as a trigger.

The location of the neutron detectors in 2004 is shown in the schematic plan view of the BLAST detector in Figure 16. The arrangement of neutron detectors was asymmetric with larger and thicker (more efficient) coverage in the right sector. This was chosen to improve the BLAST measurement of the neutron electric form factor $G_E^n$ which would be more sensitive to neutrons scattering into the right sector once the deuteron spin vector was chosen to be directed horizontally into the left sector. The L20 walls tripled the effective detector thickness of the Ohio wall at low $Q^2$ between 45–90°. The L15 walls provided

[8] Hamamatsu, Bridgewater, NJ, USA

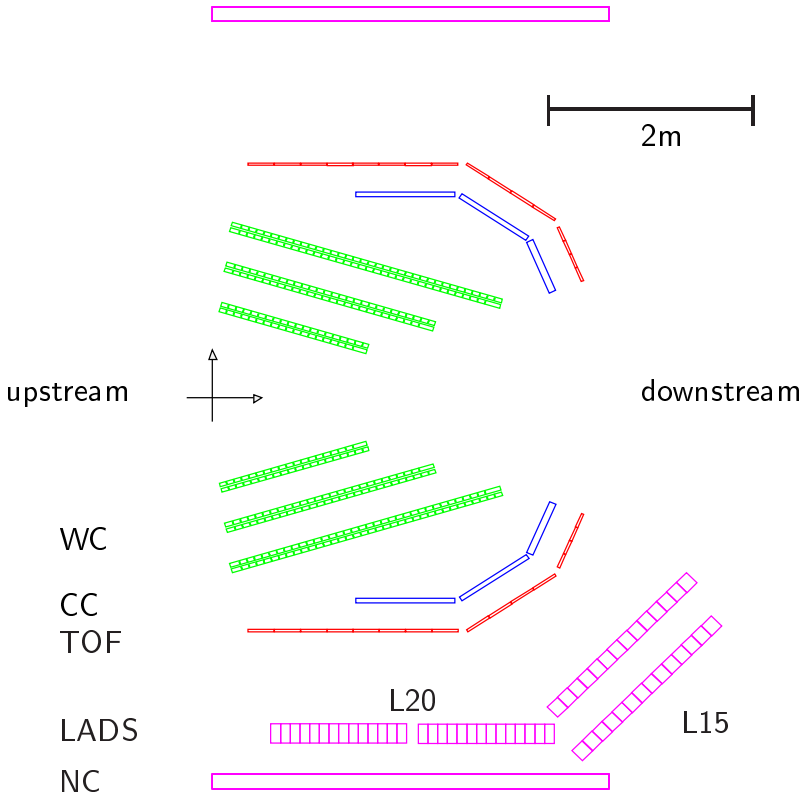


Figure 16: Schematic plan view of the BLAST detector configuration during the 2004 running period.

30 cm of total thickness in the high $Q^2$ region between 25–45°. In 2005 the left sector Ohio wall was moved forward to cover 30–80°.

During running in 2004 it was observed that gammas originating at the collimator upstream of the BLAST target generated high rates which tripped the most forward LADS bars. To reduce this rate, 3/8 inch lead sheets were mounted in front of the L15 detectors. In 2005, 1 inch iron plates were installed in front of the L15 detectors which acted as both a shield against low energy photon showers and as a converter for high energy neutrons, enhancing the neutron detection efficiency.

*4.6. Backward Angle TOF (BAT) Detector*

In order to detect electrons scattered at angles between 90° and 110° a large (12 PMTs) Čerenkov box (see 4.3) and four scintillator bars identical to the large angle TOFs (see 4.4) were mounted at backward angles in both left and right sectors. These detectors were not combined with any tracking detector nor backed up with neutron detectors. However, often the scattered proton could be detected in the main detector and kinematic information determined from the proton's scattering angle and momentum could be correlated with events in the BATs to select *ep* elastic scattering. Thus the BAT detectors were able to extend the coverage of BLAST for some reaction kinematics.

*4.7. Laser Flasher System*

A laser flasher system was used to monitor the timing of all photomultiplier based detector systems. A Spectra-Physics[9] model VSL-337ND-S ultraviolet nitrogen laser was used. The laser output was split into numerous, equal length fiber optic cables and connected to the centers of each scintillator bar or Čerenkov box. The laser output was attenuated to be within the ADC range for each detector. A flasher trigger for the data acquisition system was generated by connecting a fiber to a photodiode.

Timing calibration measurements were carried out using the laser flasher system. Since flasher events occur simultaneously in all detectors, the position of the flasher peak in the TDC is a measure of the offset introduced by the TDC device and by the length of cables and processing times.

The laser was pulsed at approximately 1 Hz during data taking and the data acquisition system recorded a FLASHER event for all detector components. These events could be analyzed to track changes in the timing of any detector channel with time. Since all scintillator bars were read out at both ends and each Čerenkov box had several PMTs, the flasher data could also be used to determine the relative time offsets between signals within a detector.

[9]Spectra-Physics, Mountain View, CA, USA

In the case of a leading-edge discriminator, the change in time with signal amplitude (walk) could also be calibrated by varying the amplitude of the laser signal. By correlating the ADC and TDC spectrum for each channel the walk effect could be accounted for on an event-by-event basis.

The timing offsets determined with the flasher were subject to drifts over long periods of time due to variations in the laser strength or when the light fibers were moved. The relative offset between pairs of scintillators were periodically generated by measuring the time correlation of cosmic ray events. Between these dedicated cosmic ray measurements the flasher-triggered data were used to monitor the timing offsets on a run-by-run basis.

*4.8. Electronics*

The amplifier/discriminator cards used on the drift chambers produced an ECL signal for each sense wire. A shielded, 32 conductor, twisted pair cable was used to carry these signals. The front end electronics for each scintillator and Čerenkov detector consisted of the photomultiplier tube bases which produced an analog signal for each channel. These signals were transported to the data acquisition and trigger electronics via RG58 coaxial cables. All these cables were approximately 45 m in length though the cables used for the wire chambers were made as short as possible to minimize attenuation. The analog PMT signals were attenuated by approximately a factor of two.

The data acquisition and trigger electronics were situated in the "D" tunnel near the BLAST experiment. This area could be accessed while the experiment was running to examine signals, check timing, or diagnose and fix problems with the electronics. The detector high voltage supplies were also housed here.

The drift chamber ECL signal cables were directly connected to LeCroy[10] 1877S TDCs located in BiRa[11] Fastbus crates. One Fastbus crate was used for each sector of BLAST.

[10] LeCroy Corp., Chestnut Ridge, NY, USA
[11] BiRa Systems, Albuquerque, NM

The signal from each scintillator PMT was sent through a passive analog splitter. Signals from the PMTs for each Čerenkov box were first combined using a CAEN[12] N402 analog adder and the output was then sent to a splitter. For each splitter, one of the outputs was sent as a prompt signal to the trigger logic electronics while the other was delayed by approximately 500 ns using an analog delay chip in a passive delay chip[13] and connected to ADCs (LeCroy 1881) in the Fastbus crates.

### *4.9. Trigger*

The trigger system used at BLAST was based on a similar design for the Jefferson Laboratory Hall A twin high resolution spectrometers, redesigned for the BLAST experiment. A schematic for the detectors in one sector is shown in Figure 17.

The prompt signals from the TOF and BAT detectors were sent to LeCroy constant fraction discriminators, CFDs, while those from the Čerenkov detectors went to LeCroy leading edge discriminators, LEDs, and those from the neutron detectors went to leading edge discriminators designed at MIT-Bates. Outputs from each discriminator were connected to scalers and to LeCroy 1875 TDCs in the Fastbus crates after appropriate delays in a PEC delay module to ensure proper timing. In addition, pairs of discriminator outputs, corresponding to the top and bottom (or left and right) PMTs of the TOF or neutron detectors, were connected to AND logic modules to generate a coincidence signal.

Outputs from the AND units were passed to a Memory Lookup Unit, MLU, for each sector which could be programmed to require different combinations of input signals to produce an output. Since the MLU only allowed 16 inputs it was necessary to combine some of the AND outputs. The ANDs of the four most forward TOF detectors were used separately but the remaining 12 TOFs (in the sector) were combined in pairs in an OR unit to produce 6 inputs to

[12]CAEN Technologies, Inc., Staten Island, NY, USA
[13]Paulus Engineering Co., London, TN

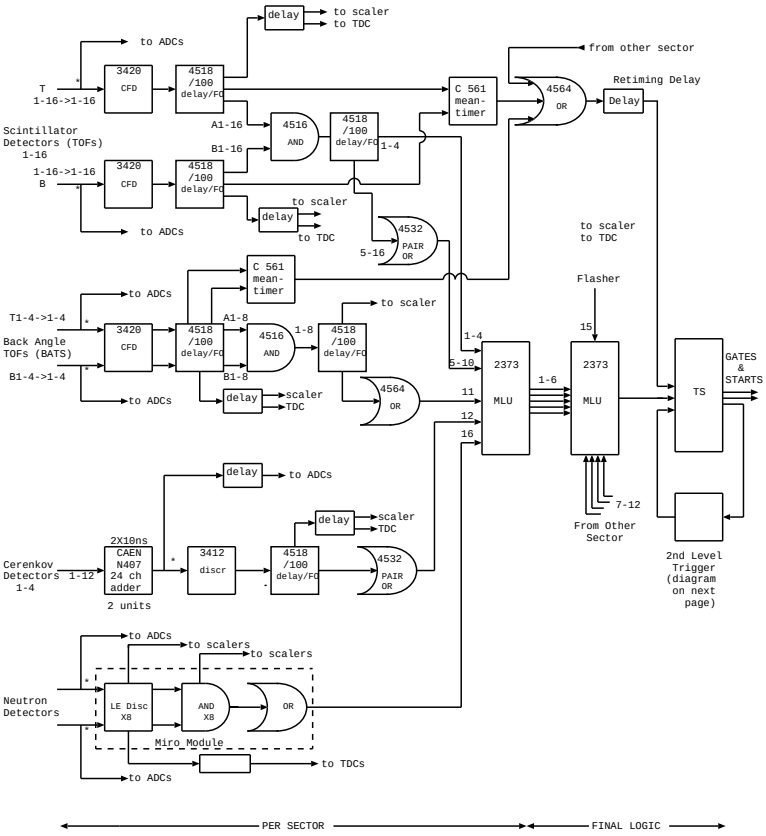


Figure 17: Schematic diagram for the BLAST trigger system.

the MLU. All Čerenkov detectors in a sector were OR'ed to provide a single MLU input. Similarly the ANDs of the four BAT TOF detectors were OR'ed to form another input and the AND of all neutron detector signals in a sector were OR'ed and formed another MLU input. The MLU for each sector produced six programmable outputs. These six outputs from each sector were then combined in a "cross" MLU, XMLU, which also accepted the flasher signal as a thirteenth input.

By programming which inputs to the sector MLUs produced which outputs and similarly programming the XMLU, the BLAST trigger could be programmed to recognize 8 classes of events, which roughly selected the event

characteristics of interest for the experiment.

Output from the XMLU was passed to the Trigger Supervisor, TS, custom designed and built by Jefferson Laboratory. The TS also received as input a trigger timing signal and a signal from the second level trigger logic described below. The TS was responsible for producing the COMMON START or COMMON STOP (drift chamber) to the TDCs and the gate to the ADCs for readout. The TS also communicated with the data acquisition system when an event was ready to be read out. It was also possible to apply prescale factors to the various event types with the TS.

In order to provide a trigger timing signal related to the time of the event at the target, the signals from the various TOF detectors were delayed as described in section 4.4. In the trigger logic the discriminated TOF signals for the top and bottom PMTs were sent to a meantimer which produced an averaged time, independent of where the particle struck along the length of the TOF scintillator bar. The OR of the meantimes of all the TOFs in both sectors was connected to the trigger supervisor and used to define the timing for the data acquisition gates and common starts and stops for the TDCs.

A second level trigger (shown in Figure 18) was formed from outputs on the

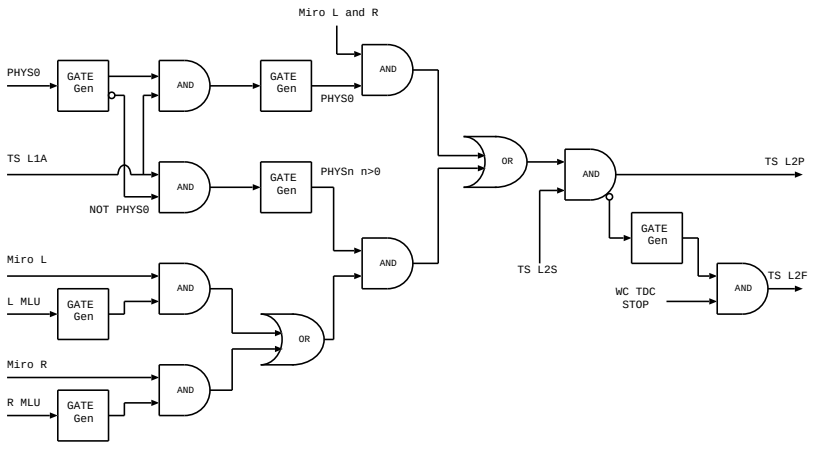


Figure 18: Schematic diagram for the BLAST second level trigger.

back of the LeCroy 1877S TDCs used by the drift chamber. This hit information was combined in specially designed logic boards to identify events which had good tracking information by requiring at least one hit in each of the three drift chambers in a sector which also had a TOF hit (*i.e.* a charged particle). This signal was one of the inputs to the trigger supervisor and reduced the trigger rate by approximately a factor of ten and removed a large number of random or noise events from the data stream.

### *4.10. Data Acquisition System*

Motorola MV162 (2004) and PowerPC (2005) single-board computers in each of the Fastbus crates served as readout controllers, ROCs, for each crate. Each ROC was a Motorola MVME5110-2263 Power PC running VxWorks 5.4 and connected to the BLAST data acquisition system via Ethernet and was based in a Struck[14] VME to Fastbus Interface.

BLAST used the CEBAF Online Data Acquisition system, CODA, developed at Jefferson Laboratory. CODA consists of several components which handle the various stages in data acquisition. When the trigger supervisor indicated a valid event, CODA read the ADCs and TDCs via Ethernet through the ROCs and passed the data to the event builder, EB. The event builder assembled the data and verified that each piece came from the same trigger. From the EB, data were passed to event transport, ET, which added other data streams such as scaler, slow control, and Compton polarimeter information. The ET also permitted the data to be monitored by sampling (spying) a fraction of the events which could be analyzed online. The event recorder, ER, wrote the data to disk.

A graphical user interface to CODA called Run Control allowed the user to establish communication with the ROCs, set trigger configurations, start and stop runs, and monitor event rates and sizes.

Buffered readout of the BLAST detector occurred at event rates up to

[14]Struck Innovative Systeme, Hamburg, Germany

1.4 kHz (0.2–0.8 kHz typical) with an event size of $\sim$ 1.5 kB. Typical deadtime was less than 10%. Online analysis programs used ET to access a sample of events and display histograms of raw ADC and TDC information and calculated quantities such as event vertex.

Struck SIS 3600 scalers were used to count hits in the various PMTs, as well as rates for the various event types. The scaler modules were located in a VME crate, along with an SIS 3800 input register that recorded status bits indicating ABS target species and polarization as well as the electron beam helicity. The scalers were read out at 1 Hz by a stand-alone program which supplied these data to the ET and to a visual display. The Computer Automated Measurement and Control, CAMAC interface was also located in this VME crate.

### *4.11. Slow Control System*

In addition to the detector electronics, trigger, and data acquisition system, successful operation of the BLAST experiment relied on numerous other components which had to be controlled, monitored, and recorded. These included the high voltages for the PMTs and drift chambers, low voltage power supplies, the gas system for the drift chambers, pressures and temperatures in the drift chambers and ABS, the electron beam current in the ring, event rates in the beam halo monitors, the Compton polarimeter, etc. These diverse components and bits of information were all organized using the Experimental Physics and Industrial Control System, EPICS[15].

EPICS is a set of software tools and applications which can be run on almost any computer to provide an infrastructure for building a distributed control system. Such systems typically comprise numerous computers, networked together to allow communication, control, and feedback of the devices connected to each computer. The EPICS system used at BLAST was integrated with the data acquisition system and the slow control data was written as part of the normal event stream and thus readily available during the analyses.

[15] http://www.aps.anl.gov/epics/index.php

## 5. Operation

During normal operation the accelerator, target, detector, and data acquisition operated automatically, requiring very little human intervention. When the current in the storage ring dropped below a preset limit, a signal would instruct the data acquisition system to stop taking data and to ramp down the high voltage on all detector components. Once the high voltages were at safe levels, the beam in the storage ring would be dumped and a new injection started. After sufficient current was again stored in the ring, the experiment would ramp up the high voltage and data taking would resume. This process can be seen graphically in Figure 19. Typically, the experimental down-time during this

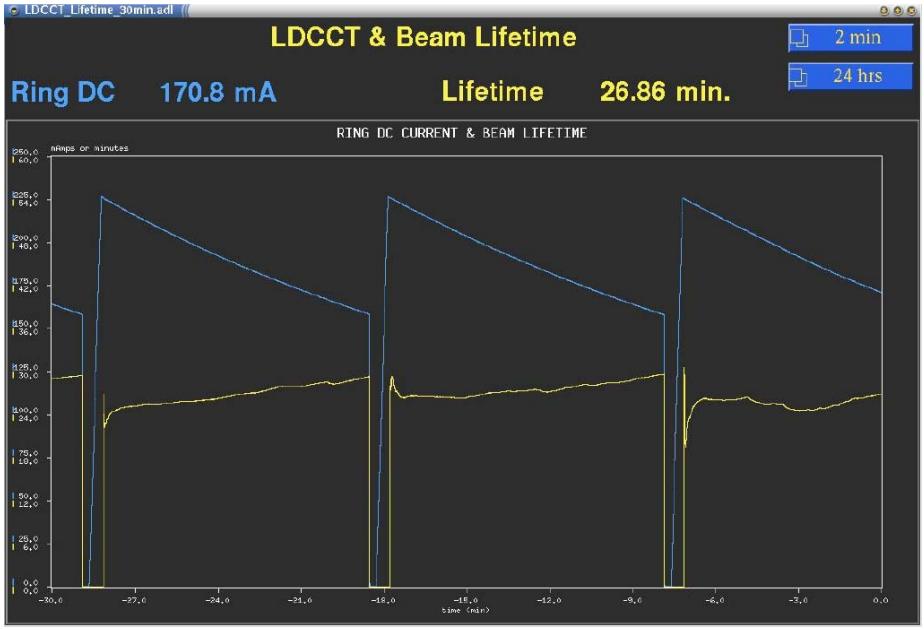


Figure 19: Plot of stored beam current (upper curves) and lifetime (lower curves) over a 30 minute period showing three successive beam fills. The typically fill shown starts with 225 mA and ends with 165 mA of stored beam while the electron beam lifetime starts at 24 minutes and gradually improves to 30 minutes.

process was about 90 seconds with data taking running for 10 minute periods. The beam helicity would be reversed for each fill. The dump current value was

chosen to maximize the integrated beam current used by the experiment.

The operation of the experiment was made significantly easier by the installation of beam quality monitors (BQM) just downstream of the BLAST target region, and by a tungsten collimator approximately 50 cm upstream from the target. The collimator served the dual purpose of protecting the target cell walls from the beam halo and helping reduce background in the wire chambers. The BQM were a set of four small scintillators with PMT readout situated symmetrically around the beampipe. These were used in tuning the beam through the target and in setting the beam scraper slits. The combined effects of the collimator, beam tuning, and selective first and second level triggers resulted in very clean events with minimal background.

The target spin states were randomly cycled independent of the beam or data acquisition with a different spin state every 5 minutes. The ABS would inhibit data acquisition for the approximately 2 seconds required for the transition.

Periodically runs were taken with the ABS switched off (*i.e.* empty target runs) to provide a measure of the background rates and processes. Similarly, an unpolarized gas system with a calibrated buffer system was used periodically to check the unpolarized asymmetries due to irregularities in the detector symmetry or efficiencies. The unpolarized system also provided a target with a known density as a check on the luminosity measurement.

Cosmic ray data were also collected and used to check relative timing between detectors. These data were generally collected during special runs on maintenance days or at times when the accelerator or target were unavailable. Cosmic events could also be distinguished within the regular data taking runs and used as well to monitor performance.

## 6. Summary

Between 2003 and 2005 the BLAST experiment successfully took data at the MIT-Bates Linear Accelerator Center. The experiment used a highly-polarized (66% typical) electron beam of 850 MeV stored in the South Hall Ring. The

polarization in the ring was monitored on-line using a Compton polarimeter. An atomic beam source provided highly-polarized internal gas targets of hydrogen ($P_Z \approx 83\%$) and deuterium ($P_Z \approx 89\%$ (79%) and $P_{ZZ} \approx 69\%$ (55%) in 2004 (2005)). A large acceptance, symmetric detector system based on a toroidal magnetic spectrometer with drift chambers for tracking, aerogel Čerenkov detectors for electron/pion discrimination, time-of-flight scintillators for triggering and relative timing, thick scintillators for neutron detection and a flexible trigger and data acquisition system was used to study numerous reaction channels simultaneously. The experiment was explicitly designed and operated to minimize systematic errors by being left/right symmetric and by frequently reversing the beam helicity and target spin states.

The analyses of the data collected by the BLAST experiment concentrate on asymmetry measurements and are therefore insensitive to the beam intensity and target densities and have reduced uncertainties due to detector efficiencies. These analyses are providing improved measurements for neutron [25, 26, 27, 28], proton [29, 30, 31], and deuteron [21, 32] form factors and allow the spin-dependent electromagnetic interaction on few-nucleon systems [33, 34] to be studied in a systematic manner.

This paper has provided a technical description of the accelerator, internal target, detector, electronics, and operation of the BLAST experiment. A future paper will detail the calibration, reconstruction, and performance of the detector.

## 7. Acknowledgments

The successful design, construction, and operation of the BLAST experiment would not have been possible without the research and technical support staffs of all the institutions involved. In particular we would like to acknowledge the MIT-Bates accelerator group for providing the high quality electron beam delivered to the experiment and the MIT-Bates research and engineering support groups for assembling and maintaining the detector and necessary infrastructure

over the many years. We would also like to acknowledge Prof. W. Haeberli for his advice and support with the internal gas target.

## References

[1] R. Alarcon, R. Milner (Eds.), Electronuclear Physics with Internal Targets and the BLAST Detector, World Scientific, Singapore, 1998, proceedings, 2nd Workshop, Cambridge, USA, May 28-30.

[2] BLAST Collaboration, BLAST Technical Design Report, Tech. rep., MIT-Bates Linear Accelerator Center (1997).

[3] D. T. Spayde, et al., Parity Violation in Elastic Electron-Proton Scattering and the Proton's Strange Magnetic Form Factor, Phys. Rev. Lett. 84 (6) (2000) 1106–1109. arXiv:nucl-ex/9909010.

[4] T. M. Ito, et al., Parity-Violating Electron Deuteron Scattering and the Proton's Neutral Weak Axial Vector Form Factor, Phys. Rev. Lett. 92 (10) (2004) 102003. arXiv:nucl-ex/0310001.

[5] E. Beise, M. Pitt, D. Spayde, The SAMPLE Experiment and Weak Nucleon Structure, Progress in Particle and Nuclear Physics 54 (1) (2005) 289–350.

[6] Z. Zhou, et al., Performance of a Compact Detector Package for the Out-of-Plane Spectrometer System, Nuclear Instruments and Methods in Physics Research A 487 (2002) 365–380.

[7] D. T. Pierce, F. Meier, Photoemission of Spin-Polarized Electrons from GaAs, Phys. Rev. B 13 (12) (1976) 5484–5500.

[8] M. Farkhondeh, W. Franklin, E. Tsentalovich, T. Zwart, E. Ihloff, MIT-Bates Polarized Source, in: Y. Makdisi, A. Luccio, W. Mackay (Eds.), AIP Conf. Proc. 675: SPIN 2002, Vol. 675 of American Institute of Physics Conference Series, 2003, pp. 1098–1102.

[9] D. Cheever, M. Farkhondeh, W. Franklin, E. Tsentalovich, T. Zwart, High Power Diode Laser System for SHR, in: Y. Makdisi, A. Luccio, W. Mackay (Eds.), AIP Conf. Proc. 675: SPIN 2002, Vol. 675 of American Institute of Physics Conference Series, 2003, pp. 1019–1023.

[10] T. Maruyama, E. L. Garwin, R. Prepost, G. Zapalac, Electron-Spin Polarization in Photoemission from Strained GaAs Grown on $GaAs_{1-x}P_x$, Phys. Rev. B 46 (7) (1992) 4261–4264.

[11] M. Farkhondeh, E. Tsentalovich, T. Zwart, E. Ihloff, New Results from the MIT-Bates Polarized Source and the Test Beam Setup, in: K. Hatanaka, T. Nakano, K. Imai, H. Ejiri (Eds.), AIP Conf. Proc. 570: SPIN 2000, Vol. 570, 2001, p. 955.

[12] T. Zwart, et al., Transmission Polarimetry at MIT Bates, in: Y. Makdisi, A. Luccio, W. Mackay (Eds.), AIP Conf. Proc. 675: SPIN 2002, Vol. 675 of American Institute of Physics Conference Series, 2003, pp. 1011–1015.

[13] T. Zwart, E. Booth, F. Casagrande, K. Dow, M. Farkhondeh, W. Franklin, E. Ihloff, K. Jacobs, J. Matthews, R. Milner, T. Smith, C. Tschalaer, E. Tsentalovich, W. Turchinetz, F. Wang, Polarized Electrons at Bates: Source to Storage Ring, in: American Institute of Physics Conference Series, Vol. 588 of American Institute of Physics Conference Series, 2001, pp. 343–349.

[14] W. A. Franklin, The MIT-Bates Compton Polarimeter for the South Hall Ring, in: 16th International Spin Physics Symposium (SPIN 2004), Trieste, Italy, 2004, p. 714.

[15] D. P. Barber, et al., The HERA Polarimeter and the First Observation of Electron Spin Polarization at HERA, Nucl. Instrum. Meth. A 329 (1-2) (1993) 79–111.

[16] I. Passchier, et al., A Compton Backscattering Polarimeter for Measuring

Longitudinal Electron Polarization, Nucl. Instrum. Meth. A 414 (1998) 446–458. arXiv:physics/9902011.

[17] V. S. Morozov, et al., Spin-Flipping Polarized Electrons, Phys. Rev. ST Accel. Beams 4 (2001) 104002.

[18] D. Cheever, et al., A Highly Polarized Hydrogen / Deuterium Internal Gas Target Embedded in a Toroidal Magnetic Spectrometer, Nucl. Instrum. Meth. A556 (2006) 410–420.

[19] M. Ferro-Luzzi, et al., Measurement of Tensor Analyzing Powers for Elastic Electron Scattering from a Polarized $^2$H Target Internal to a Storage Ring, Phys. Rev. Lett. 77 (13) (1996) 2630–2633.

[20] L. van Buuren, D. Szczerba, J. van den Brand, H. Bulten, M. Ferro-Luzzi, S. Klous, H. Kolster, J. Lang, F. Mul, H. Poolman, M. Simani, Performance of a Hydrogen/Deuterium Polarized Gas Target in a Storage Ring, Nucl. Instrum. Methods A 474 (2001) 209–223.

[21] C. Zhang, Measurement of Tensor Analyzing Powers in Elastic Electron Deuteron Scattering with BLAST, Ph.D. thesis, Massachusetts Institute of Technology (May 2006).

[22] K. Dow, et al., Magnetic Field Measurements of the BLAST Spectrometer, to be published.

[23] B. Tonguc, R. Alarcon, T. Botto, J. Calarco, A. Degrush, O. Filoti, E. Geis, J. Kelsey, J. Prince, E. Six, C. Vidal, The BLAST Cherenkov detectors, Nucl. Instrum. Methods A 553 (1-2) (2005) 364–369.

[24] T. Alteholz, et al., A Large Acceptance Detector System (LADS) for Studies of Pion Absorption, Nucl. Instrum. Meth. A373 (1996) 374–386.

[25] V. Ziskin, Measurement of the Electric Form Factor of the Neutron at Low Momentum Transfers Using a Vector Polarized Deuterium Gas Target at BLAST, Ph.D. thesis, Massachusetts Institute of Technology (Apr 2005).

[26] N. Meitanis, A Measurement of the Neutron Magnetic Form Factor $G_M^n$ from Quasi-elastic ${}^2\vec{H}(\vec{e}, e')$ and low $Q^2$, Ph.D. thesis, Massachusetts Institute of Technology (Mar 2006).

[27] E. Geis, The Electric Form Factor of the Neutron at Low Momentum Transfers as Measured at Bates Large Acceptance Spectrometer Toroid, Ph.D. thesis, Arizona State University (May 2007).

[28] E. Geis, et al., The Charge Form Factor of the Neutron at Low Momentum Transfer from the ${}^2\vec{\mathrm{H}}(\vec{\mathrm{e}}, \mathrm{e}'\mathrm{n})\mathrm{p}$ Reaction, Phys. Rev. Lett. 101 (2008) 042501. arXiv:0803.3827.

[29] C. Crawford, Precision Measurement of the Proton Electric to Magnetic Form Factor Ratio with BLAST, Ph.D. thesis, Massachusetts Institute of Technology (May 2005).

[30] A. Sindile, Proton Form Factor Ratio Measurement with BLAST, Ph.D. thesis, University of New Hampshire (May 2006).

[31] C. B. Crawford, et al., Measurement of the Proton's Electric to Magnetic Form Factor Ratio from ${}^1\vec{H}(\vec{e}, e'p)$, Phys. Rev. Lett. 98 (5) (2007) 052301. arXiv:nucl-ex/0609007.

[32] P. Karpius, Vector Polarization Observables of the Deuteron and A New Measurement of the Magnetic Dipole Form Factor $G_M$, Ph.D. thesis, University of New Hampshire (Dec 2005).

[33] A. Maschinot, Analysis of Scattered Protons in Deuteron Electrodisintegration with a Polarized Electron Beam and an Internal Polarized Target, Ph.D. thesis, Massachusetts Institute of Technology (Sep 2005).

[34] O. Filoti, Inclusive Scattering of Polarized Electrons from Polarized Protons in the $\Delta$-Excitation Region with BLAST, Ph.D. thesis, University of New Hampshire (Apr 2007).